



Deposited via The University of Leeds.

White Rose Research Online URL for this paper:

<https://eprints.whiterose.ac.uk/id/eprint/144069/>

Version: Accepted Version

Article:

Gao, J, Chen, H, Chen, J et al. (2019) Explorations on the continuous oxidation kinetics of diesel PM from heavy-duty vehicles using a single ramp rate method. *Fuel*, 248. pp. 254-257. ISSN: 0016-2361

<https://doi.org/10.1016/j.fuel.2019.02.127>

(c) 2019, Elsevier Ltd. This manuscript version is made available under the CC BY-NC-ND 4.0 license <https://creativecommons.org/licenses/by-nc-nd/4.0/>

Reuse

This article is distributed under the terms of the Creative Commons Attribution-NonCommercial-NoDerivs (CC BY-NC-ND) licence. This licence only allows you to download this work and share it with others as long as you credit the authors, but you can't change the article in any way or use it commercially. More information and the full terms of the licence here: <https://creativecommons.org/licenses/>

Takedown

If you consider content in White Rose Research Online to be in breach of UK law, please notify us by emailing eprints@whiterose.ac.uk including the URL of the record and the reason for the withdrawal request.

1 Explorations on the continuous oxidation kinetics of diesel PM using single
2 ramp rate method

3 Jianbing Gao^{a,b}, Haibo Chen^{b,*}, Junyan Chen^b, Chaochen Ma^{a,*}, Guohong Tian^c, Ying Li^d

4 a. School of Mechanical Engineering, Beijing Institute of Technology, Beijing 100081, China

5 b. Institute for Transport Studies, University of Leeds, Leeds LS2 9JT, UK

6 c. Department of Mechanical Engineering Sciences, University of Surrey, Guildford GU2 7XH, UK

7 d. WOCH Ltd, Castleford WF10 5TH, UK

8

9

10 * Corresponding author:

11 Chaochen Ma

12 E-mail:machaochen1900@163.com

13 Haibo Chen

14 E-mail: H.Chen@its.leeds.ac.uk

15 **Abstract**

16 Particulate matter (PM) emitted by internal combustion engines has brought about serious environmental
17 problems. Investigations of the PM oxidation behaviors and kinetics make the foundations of decreasing
18 PM emission and working out the regeneration problems of PM capture devices. In this paper, the
19 oxidation kinetics and microstructure evolutions of diesel PM in the oxidation process were researched.
20 The results showed that thermogravimetric analysis (TGA) temperature history had a limited influence on
21 the tendency of the oxidation kinetics. The volatilization of the organic compounds dominated the mass
22 loss without any heat release at the initial stage of PM oxidation. The abnormal phenomenon (negative
23 apparent activation energy) was observed in the oxidation process when the oxidation temperature was in
24 the range of 200°C~ 340°C, which was ubiquitous during PM oxidation. However, the abnormal
25 phenomenon disappeared if the PM sample was pre-treated to remove the volatile organic compounds
26 (VOC), with the result that the phenomenon was caused by the VOC. The hydrogen bonding complex
27 was formed in that temperature range, where the energy of the hydrogen bonding complex was lower than
28 the value of the reactants, which caused the negative apparent activation energy. The apparent activation
29 energy increased gradually when the temperature was higher than 340°C.

30 **Keywords:** diesel particulate matter; oxidation kinetics; microstructure evolutions; negative activation
31 energy

32 **1. Introduction**

33 Large amounts of diesel particles were emitted into the atmosphere, which had a huge potential impact on
34 the environment. Ammann's results [1] showed that the heterogeneous production of HNO₂ from NO₂
35 suspending on soot particles was 10⁵~10⁷ times faster than previously reported surface suspending
36 reactions, which implied that soot particles also promoted the formation of photochemical smog.
37 Michelsen et. al [2] reviewed the soot formation, evolutions and oxidation, with the results that the active
38 radicals (such as OH, O, CH and CH₂) played a vital role at the initial stage of soot formation process.
39 Meantime, the soot agglomerates and graphitic aggregates happened, which resulted in the stable soot
40 particles. Deeply investigating the PM oxidation behaviors and oxidation kinetics contributed to
41 decreasing the PM emission and to optimizing the PM removal devices, such as diesel particulate filters
42 (DPFs) [3] and non-thermal plasma (NTP) reactors [4].

43 PM nanostructures of a light-duty diesel engine [5], the effect of exhaust gas recirculation (EGR) on PM
44 oxidation activity [6], diesel PM oxidation behaviors [7, 8], and PM oxidation model [9] were widely

45 investigated. Vander Wal et.al [10] quantified the soot nanostructures using fringe separation distance,
46 fringe length and tortuosity, which revealed the relations of the soot nanostructures and PM formation
47 temperature. Further, the influence of the heat-treatment temperature on the soot nanostructures was
48 investigated that the crystallites were more orderly arranged after heat-treatment [11]. The statistics of the
49 primary particle diameters were made based on the soot morphology, which showed closely related to
50 oxidation activity [12], that the average value was between 20 nm and 25 nm. Qu et. al [13] investigated
51 the oxidation activity of biodiesel PM, which presented closely related to the oxygen and VOC contents
52 of biodiesel PM. López-Fonseca et. al [14] calculated the oxidation kinetics using different reaction
53 models, with the conclusions that the choose of the reaction models significantly influenced the oxidation
54 activity. The commonly used methods to calculate the PM oxidation kinetics were based on single ramp
55 rate and multi-ramp rate thermogravimetric analysis (TGA) profiles using Arrhenius equation [4, 15, 16].
56 Multi-ramp rate method in this paper was that at least three TGA profiles obtained at different ramp rates were
57 needed to calculate the oxidation kinetics. Sharma et. al [15] investigated the oxidation kinetics using
58 single ramp rate method that the activation energy was almost the same in a small temperature range. The
59 samples used for the TGA experiments were raw PM or pre-treated PM at high temperature,
60 non-oxidizing atmosphere. As for the raw PM, the oxidation and volatilization happened simultaneously
61 for volatile organic compounds (VOC) contained in the diesel PM, which led to the distortions of the
62 oxidation kinetic lines. The oxidation kinetic lines were missed at the low temperature regions if PM
63 samples were pre-treated at high temperature atmosphere to remove the VOC; also, high temperature
64 pre-treatment significantly decreased the oxidation activity. The differential scanning calorimetry (DSC)
65 device detected the heat release rate as the function of oxidation temperature [4]. This method effectively
66 detected the PM oxidation temperature and oxidation intensity at low temperature regions based on the
67 heat loss during oxidation. The single ramp rate method presented the oxidation kinetic changes
68 continuously in the oxidation process. The oxidation kinetic calculations using DSC profiles based on the
69 single ramp rate method was seldomly reported to the authors' knowledge. As can be seen from the
70 references [17, 18], the details of the oxidation kinetics based on multi-ramp rate method were neglected
71 due to the large temperature intervals. The oxidation kinetics based on the single ramp rate method in
72 references [19, 20] were only focused on the high temperature zones.

73 In this paper, the TGA and DSC profiles were combined to investigate the PM oxidation kinetics in the
74 whole oxidation process. The single ramp rate method was used to research the details of the oxidation

75 kinetics. The sketches of microstructure evolutions in PM oxidation process were assisted to clarify PM
76 oxidation kinetics. With emphasis, the non-reported abnormal phenomenon of diesel PM oxidation
77 kinetics in the oxidation process was discovered and analyzed.

78 **2. Oxidation kinetics lines extraction**

79 Calculations of the oxidation kinetics using oxidation profiles is based on Arrhenius equation (Equation 1)
80 and its transformation is as Equation 2,

$$81 \quad k = A \exp\left(-\frac{E}{RT}\right) \quad (1)$$

$$82 \quad -\frac{dm}{dt} = km^n p_{O_2}^r = A \exp\left(-\frac{E}{RT}\right) m^n p_{O_2}^r \quad (2)$$

83 Where m , t , k , n , p_{O_2} , r , A , E , R , T are sample mass, time, reaction rate constant, reaction order for carbon,
84 partial pressure of oxygen, reaction order for oxygen, pre-exponential factor, apparent activation energy,
85 universal gas constant (8.314 J/mol·K) and temperature. References [15, 21] showed that the reaction
86 orders of different soot were close to unit (1.0). So that Equation 2 is transferred into Equation 3,

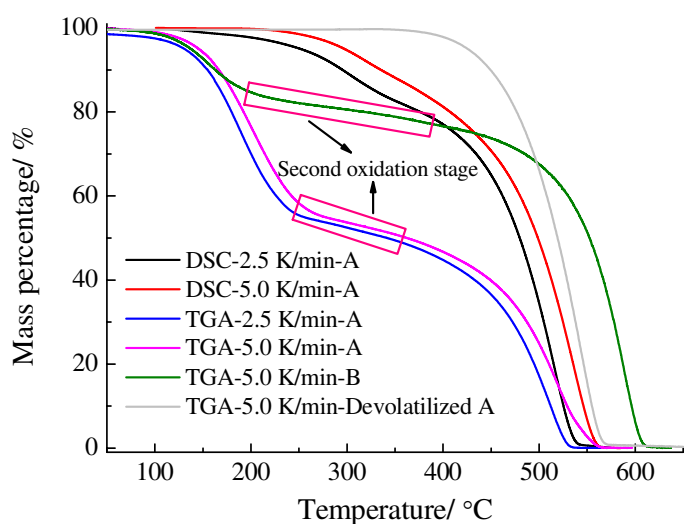
$$87 \quad \ln\left(-\frac{dm}{m \cdot dt}\right) = \ln\left(A p_{O_2}^r\right) - \frac{E}{RT} \quad (3)$$

88 In the oxidation process of a narrow temperature range, $\ln(-dm/(m \cdot dt))$ shows a linear correlation with
89 $-1/(R \cdot T)$. E and A could be calculated from the slope and intercept of Equation 3. In the oxidation process,
90 the slope and intercept changed gradually, resulting from the changes of the physicochemical properties,
91 including ingredients (such soot, SOF and salts), structures, oxygen contents [4, 22].

92 **3. TGA and DSC profiles**

93 In order to decrease the experimental errors, vacant combustion in air was performed to remove the
94 residuals before TGA and DSC experiments. The duplicate tests of TGA experiments are shown in Figure.
95 S1. As can be seen, the repeatability of the experiments is excellent. The calculations of oxidation kinetic
96 lines were based on TGA and DSC profiles. The oxidation profiles based on TGA and DSC experiments
97 are shown in Figure 1, and parts of these curves were reported in reference [4]. Diesel PM samples A and
98 B were collected at 60% and 80% engine load conditions, respectively. Devolatilized sample A was
99 obtained by pre-treating sample A at high temperature, non-oxidizing atmosphere, the pre-treatment
100 process was as the following: sample A was heated from room temperature to 450 °C at a 20 °C/min ramp
101 rate in N₂ atmosphere and was kept at 450 °C isothermal condition for 15 minutes; Then, it was cooled to

102 atmosphere temperature. The DSC profiles were obtained by the normalization of the heat release curves,
103 in which the assumption was made that the heat release rate was proportional to the PM mass loss rate
104 caused by oxidation (rather than the volatilization). The detailed discussions about the TGA and DSC
105 profiles were presented in reference [4]. Reference [13] indicated that oxidation and volatilization
106 happened simultaneously when the temperature was lower than 350 °C, which was similar to the authors'
107 research. Also, reference [19] defined the mass loss caused by low volatility and high volatility which
108 were in the ranges of 200 °C~500 °C and 40 °C~200 °C, respectively. Advanced technologies should be
109 adopted to further clearly distinguish the oxidation and volatilization. This paper was mainly focused on
110 the details of the oxidation kinetics during PM oxidation.

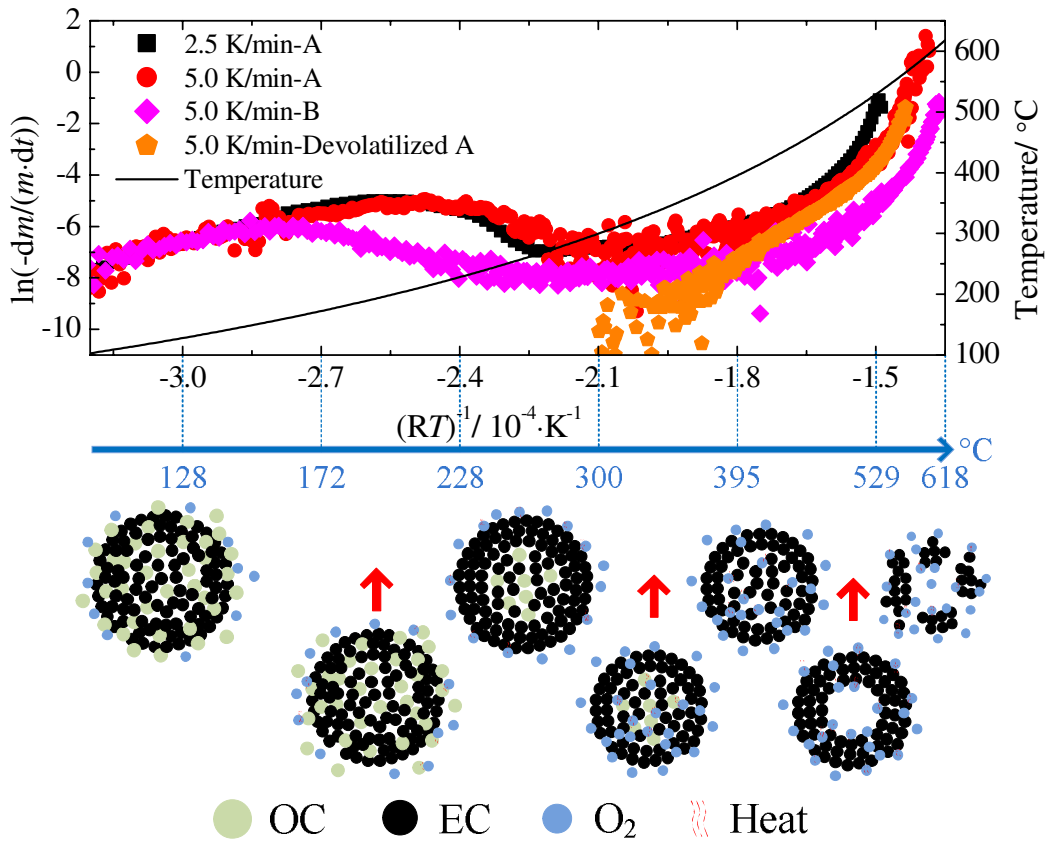


111
112 Figure 1 Diesel PM oxidation profiles based on TGA and DSC experiments [4]

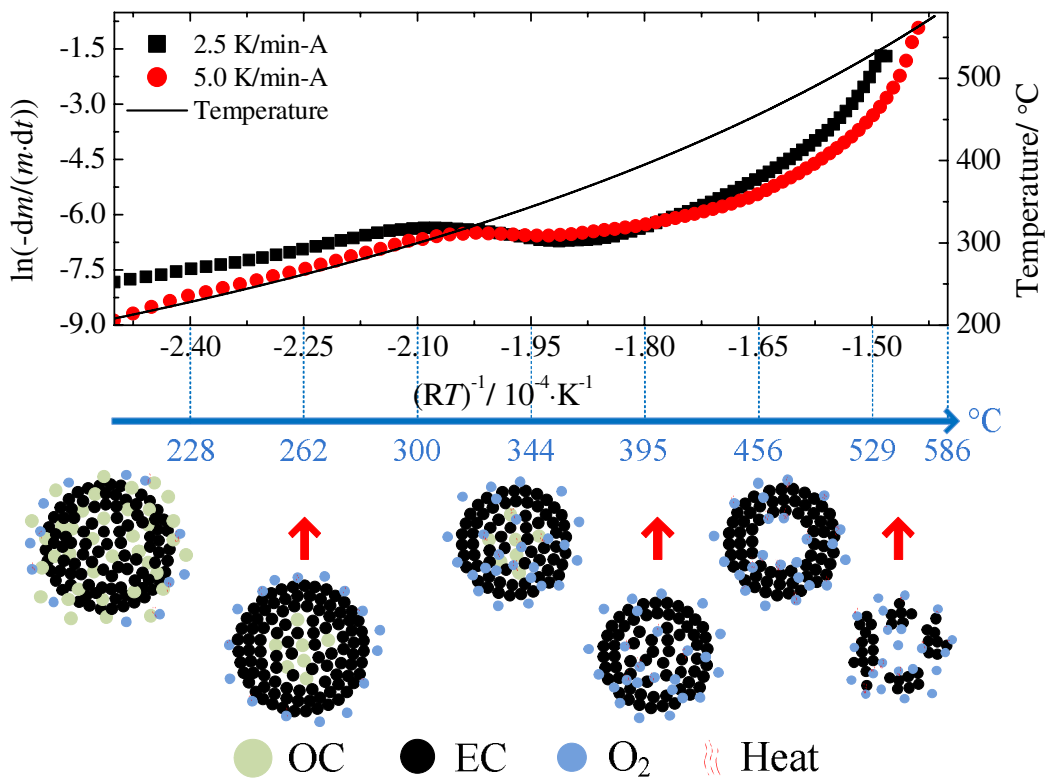
113 4. Oxidation kinetics analysis

114 Details of the oxidation kinetics in the oxidation process were neglected if the multi-ramp rate method
115 was used due to the temperature intervals, as showed in references [4, 18]. However, the oxidation
116 kinetics based on the single ramp rate method was continuous, which could clearly indicate the details in
117 the whole oxidation process. Figure 2 shows the oxidation kinetic lines and microstructure evolutions in
118 the oxidation process. Based on the microstructure evolutions, the phenomenons in the oxidation process
119 could be more clearly clarified. The slopes of the oxidation kinetic lines reflected the apparent activation
120 energy [23]. The tendency of the apparent activation energy in the oxidation process was similar at
121 different ramp rate conditions for DSC based method, as shown in Figure 2(b). Similarly, the ramp rates
122 had a small influence on the tendency of apparent activation energy for TGA based method (Figure 2(a)).
123 Apparent activation energy was almost the same when the oxidation temperature was lower than 310 °C;

124 then, it dropped to below zero around 344 °C and increased gradually in the following oxidation process
125 for the DSC based method. Compared with the TGA based oxidation kinetic lines, the DSC based kinetic
126 lines were smoother due to the fact that the DSC device tested the heat release free of the vibration and
127 noise effects. The differences of the apparent activation energy tendency for the TGA and DSC methods
128 were mainly focused on the low temperature regions, where the temperature was lower than 344 °C (it
129 was exemplified using sample A at 5.0 °C/min ramp rate). The apparent activation energy changed little
130 when the temperature was lower than 200 °C, where the volatilization dominated the mass loss; then, it
131 decreased in the temperature ranges of 200 °C~344 °C. The tendency was the same by comparing
132 samples A and B, while the differences were mainly focused on the characteristic temperatures, such as
133 the temperature where the transitions of the apparent activation energy happened. For the pre-treated PM
134 sample (devolatilized A), the apparent activation energy was almost the same in the temperature range of
135 340 °C~530 °C, where the oxidation dominated the reactions; it increased rapidly after that temperature
136 range. It seemed that the pre-treatment at non-oxidizing atmosphere had a small effect on the apparent
137 activation energy at high temperature zones. Reference [15] calculated the diesel soot oxidation kinetics
138 using single ramp rate method that the apparent activation energy was almost kept at the same value in
139 the temperature range of 515 °C~635 °C. The phenomenon was similar to the devolatilized PM in this
140 paper. Wang et. al [19] indicated that the changes of the apparent activation energy in the oxidation
141 process using single ramp rate method were much smaller for low ramp rate than that of high ramp rate in
142 the temperature range of 410 °C~525 °C.



(a) Oxidation kinetic lines based on TGA profiles and microstructure evolutions



(b) Oxidation kinetic lines based on DSC profiles and microstructure evolutions

Figure 2 Oxidation kinetic lines and microstructure evolutions: OC, organic carbon; EC, element carbon

148 Sample A (5.0 K/min ramp rate) was taken as the example to detailed illustrate the oxidation kinetic
149 phenomenon in the oxidation process. For the TGA based method, the apparent activation energy was
150 nearly a constant value when the temperature was lower than 200 °C, however, the volatilization
151 dominated the reaction at the temperature region as indicated in DSC profiles (Figure 1). This
152 phenomenon was similar to the results in the reference [24]. Actually, the apparent activation energy in
153 the region was the energy that was needed to volatilize the low molecular VOC contained in the diesel
154 PM. As shown in the microstructure evolutions in Figure 2(a), only the surface VOC volatilization
155 happened at this stage. Chemical reactions happened for VOC when the temperature was higher than
156 200 °C. While the chemical reactions dominated mass loss when temperature was higher than 250 °C,
157 which could be gotten by comparing the TGA and DSC based oxidation profiles. In the temperature zone,
158 chemical reactions and volatilization happened simultaneously with heat release. Soot surfaces were
159 oxidized gradually with the following results that the oxidation was transferred from the surfaces to inner
160 cores at high temperature conditions.

161 In the temperature range of 200 °C~310 °C, an abnormal phenomenon was observed that the apparent
162 activation energy calculated using TGA based profiles was the negative, however, it was positive for DSC
163 based profiles. During the temperature region, the mass loss percentage for the TGA methods was high,
164 however, the heat release was low. Pyrolysis reactions happened in this process, where the high molecular
165 VOC was broken up into low molecular VOC, whose volatilization temperature was low. The pyrolysis
166 reactions of high molecular VOC led to the rapidly decrease of PM mass. The pyrolysis reactions caused
167 the negative apparent activation energy in TGA based method, and the detailed reasons would be
168 discussed below. Much high molecular VOC was converted into low molecular VOC that most of the low
169 molecular VOC flowed out of the TGA device. Due to the high atmosphere temperature in TGA device,
170 part of low molecular VOC was oxidized once the high molecular VOC was broken up, which caused the
171 heat release during this stage. So that the TGA based kinetic lines partly depicted the pyrolysis reactions
172 of high molecular VOC during this temperature region, while it was low molecular VOC oxidation in
173 DSC based kinetic lines.

174 In the small temperature range of 310 °C~ 340 °C, the apparent activation energy was negative or around
175 zero for both the TGA and DSC based methods. The mass loss rate was low in this temperature region.
176 The abnormal phenomenon was ubiquitous during the PM oxidation, it can be known by comparing the
177 oxidation kinetic lines of samples A and B. However, the phenomenon was neglected in all the reported

178 researches about PM oxidation kinetics to the authors' knowledge [25-27]. This was mainly caused by the
179 multi-ramp rate method calculating the oxidation kinetics, and PM pre-treatment at high temperature
180 conditions. For different PM samples, the discrepancy was mainly focused on the positions and durations
181 of the abnormal phenomenon, as presented in Figure 2(a). Also, it seemed that the durations of the
182 abnormal phenomenon showed closely related to the high molecular VOC content and the second
183 oxidation phase (slow oxidation in Figure 1), which was concluded by correlating Figure 1. The low
184 molecular VOC content was almost the same for samples A and B (mass loss when temperature was
185 lower than 200 °C). Evidently, the second oxidation phase lasted a wide temperature region, which
186 resulted of the huge temperature range of the abnormal phenomenon. The abnormal phenomenon
187 disappeared when the sample was pre-treated at high temperature atmosphere to remove the VOC
188 (devolatilized sample A). So that it was concluded by comparing sample A and devolatilized sample A
189 that the abnormal phenomenon was caused by VOC. Smith et. al [28] summarized large amounts of
190 elementary reactions, with the conclusion that the apparent activation energy was negative for the
191 elementary reaction in a narrow temperature range. Also, the abnormal phenomenon in chemical reactions
192 was reported in other chemical reaction process [29-31].

193 The general chemical reactions had the positive temperature effect that the reaction rate constant
194 increased with temperature. The apparent activation energy was smaller than zero if the chemical
195 reactions were the negative temperature effect. The negative temperature effect happened in the abnormal
196 periods. It was considered that the hydrogen bonding complex was formed during the oxidation that the
197 energy of the hydrogen bonding complex was lower than the value of the reactants, which led to the
198 negative apparent activation energy [28]. Much hydrogen bonding complex was formed in the abnormal
199 temperature zone, which was the main reason leading to the low mass loss rate in the following reactions
200 despite the temperature increased continually. The reason caused the abnormal phenomenon was same for
201 the temperature range of 200 °C~310 °C in the TGA based method. After the abnormal period, the
202 apparent activation energy increased gradually with the oxidation reaction proceeding.

203 **5. Conclusions**

204 In order to get the details of the oxidation kinetics in diesel PM oxidation process, the oxidation kinetics
205 based on DSC and TGA profiles using single ramp rate method were researched. Meantime, the
206 microstructure evolutions in the diesel PM oxidation process were assisted to clearly clarify the oxidation
207 kinetics. At the initial stage of PM oxidation, VOC volatilization dominated the mass loss and no

208 chemical reactions happened. Large amounts of high molecular VOC were breakup into low molecular
209 VOC, which caused the abnormal phenomenon, negative apparent activation energy, in the temperature
210 range of 200 °C~310 °C in the TGA based method. Meantime, the oxidation of part low molecular VOC
211 released heat in that temperature range. The abnormal phenomenon was also observed in the temperature
212 range of 310 °C~340 °C, where hydrogen bonding complex, with low energy being smaller than the
213 values of reactants, was formed. In addition, the hydrogen bonding complex caused the slow oxidation
214 activity in the following reaction process. The apparent activation energy increased gradually when the
215 temperature was higher than 340 °C. The abnormal phenomenon was ubiquitous during diesel PM
216 oxidation and it disappeared after being pre-treated at high temperature conditions, which indicated that
217 the abnormal phenomenon was caused by the VOC contained diesel PM.

218

219 **Acknowledgement**

220 The research described in this paper was supported in part by the EU-funded project optiTruck (grant
221 agreement No 713788) which has the ultimate aim to develop and test a prototype ‘global 490 optimizer’,
222 capable of achieving a fuel reduction of at least 20% for 40 tonne trucks while still meeting relevant Euro
223 VI emission standards.

224

225 **Reference**

- 226 [1] Ammann M, Kalberer M, Jost D, Tobler L, Rössler E, Piguet D, et al. Heterogeneous production of
227 nitrous acid on soot in polluted air masses. *Nature* 1998;395(6698):157.
- 228 [2] Michelsen H. Probing soot formation, chemical and physical evolution, and oxidation: A review of in
229 situ diagnostic techniques and needs. *Proceedings of the Combustion Institute* 2017;36(1):717-35.
- 230 [3] Jiao P, Li Z, Shen B, Zhang W, Kong X, Jiang R. Research of DPF regeneration with NO_x-PM
231 coupled chemical reaction. *Appl Therm Eng* 2017;110:737-45.
- 232 [4] Gao J, Ma C, Xing S, Sun L. Oxidation behaviours of particulate matter emitted by a diesel engine
233 equipped with a NTP device. *Appl Therm Eng* 2017;119:593-602.
- 234 [5] Vander Wal RL, Strzelec A, Toops TJ, Daw CS, Genzale CLJF. Forensics of soot: C5-related
235 nanostructure as a diagnostic of in-cylinder chemistry. 2013;113:522-6.
- 236 [6] Al-Qurashi K, Boehman AL. Impact of exhaust gas recirculation (EGR) on the oxidative reactivity of
237 diesel engine soot. *CoFl* 2008;155(4):675-95.

- 238 [7] Strzelec A, Toops T, Daw C, Foster DE, Rutland C. SAE Technical Paper 2010-01-2127,
239 <https://doi.org/10.4271/2010-01-2127>, SAE 2010 Powertrains Fuels & Lubricants Meeting.
- 240 [8] Jaramillo IC, Gaddam CK, Vander Wal RL, Lighty JS. Effect of nanostructure, oxidative pressure
241 and extent of oxidation on model carbon reactivity. *CoFl* 2015;162(5):1848-56.
- 242 [9] Lee J, Tzanetakis T, Zhang Y, Traver M, Lewis S, Moses-DeBusk M, et al. Characterization of
243 Particulate Matter Emissions from Heavy-Duty Partially Premixed Compression Ignition with
244 Gasoline-Range Fuels. SAE Technical Paper 2019-01-1185, <https://doi.org/10.4271/2017-01-0932>,
245 WCX: SAE World Congress Experience (in press).
- 246 [10] Vander Wal RL, Tomasek AJ, Pamphlet MI, Taylor CD, Thompson WK. Analysis of HRTEM
247 images for carbon nanostructure quantification. *JNR* 2004;6(6):555-68.
- 248 [11] Yehliu K, Vander Wal RL, Boehman AL. A comparison of soot nanostructure obtained using two
249 high resolution transmission electron microscopy image analysis algorithms. *Carbon*
250 2011;49(13):4256-68.
- 251 [12] Barone TL, Storey JM, Youngquist AD, Szybist JPJAE. An analysis of direct-injection spark-ignition
252 (DISI) soot morphology. 2012;49:268-74.
- 253 [13] Qu L, Wang Z, Zhang J. Influence of waste cooking oil biodiesel on oxidation reactivity and
254 nanostructure of particulate matter from diesel engine. *Fuel* 2016;181:389-95.
- 255 [14] López-Fonseca R, Landa I, Elizundia U, Gutiérrez-Ortiz M, González-Velasco J. A kinetic study of
256 the combustion of porous synthetic soot. *Chem Eng J* 2007;129(1):41-9.
- 257 [15] Sharma HN, Pahalagedara L, Joshi A, Suib SL, Mhadeshwar AB. Experimental study of carbon
258 black and diesel engine soot oxidation kinetics using thermogravimetric analysis. *Energy Fuels*
259 2012;26(9):5613-25.
- 260 [16] Darcy P, Da Costa P, Mellottée H, Trichard J-M, Djega-Mariadassou G. Kinetics of catalyzed and
261 non-catalyzed oxidation of soot from a diesel engine. *Catal Today* 2007;119(1):252-6.
- 262 [17] Meng Z, Yang D, Yan Y. Study of carbon black oxidation behavior under different heating rates.
263 *JTAC* 2014;118(1):551-9.
- 264 [18] Ma C, Gao J, Zhong L, Xing S. Experimental investigation of the oxidation behaviour and thermal
265 kinetics of diesel particulate matter with non-thermal plasma. *Appl Therm Eng* 2016;99:1110-8.
- 266 [19] Wang C, Xu H, Herreros JM, Lattimore T, Shuai S. Fuel effect on particulate matter composition and
267 soot oxidation in a direct-injection spark ignition (DISI) engine. *Energy Fuels* 2014;28(3):2003-12.

- 268 [20]Chong HS, Aggarwal SK, Lee KO, Yang SY, Seong H. Experimental investigation on the oxidation
269 characteristics of diesel particulates relevant to DPF regeneration. *CST* 2013;185(1):95-121.
- 270 [21]Stanmore BR, Brilhac J-F, Gilot P. The oxidation of soot: a review of experiments, mechanisms and
271 models. *Carbon* 2001;39(15):2247-68.
- 272 [22]Gao J, Ma C, Xing S, Sun L, Huang L. A review of fundamental factors affecting diesel PM
273 oxidation behaviors. *Science China Technological Sciences* 2018;61(3):330–45.
- 274 [23]Jung H, Kittelson DB, Zachariah MR. The influence of a cerium additive on ultrafine diesel particle
275 emissions and kinetics of oxidation. *CoFl* 2005;142(3):276-88.
- 276 [24]Wang-Hansen C, Ericsson P, Lundberg B, Skoglundh M, Carlsson P-A, Andersson B.
277 Characterization of particulate matter from direct injected gasoline engines. *ToCat* 2013;56(1-8):446-51.
- 278 [25]Karin P, Boonsakda J, Siricholathum K, Saenkhumvong E, Charoenphonphanich C, Hanamura K.
279 Morphology and oxidation kinetics of CI engine's biodiesel particulate matters on cordierite Diesel
280 Particulate Filters using TGA. *International Journal of Automotive Technology* 2017;18(1):31-40.
- 281 [26]López-Fonseca R, Landa I, Gutiérrez-Ortiz M, González-Velasco J. Non-isothermal analysis of the
282 kinetics of the combustion of carbonaceous materials. *JTAC* 2005;80(1):65-9.
- 283 [27]Alozie NS, Fern G, Peirce D, Ganippa L. Influence of Biodiesel Blending on Particulate Matter (PM)
284 Oxidation Characteristics. SAE Technical Paper 2017-01-0932, <https://doi.org/10.4271/2017-01-0932>,
285 WCX™ 17: SAE World Congress Experience.
- 286 [28]Smith IW, Ravishankara A. Role of hydrogen-bonded intermediates in the bimolecular reactions of
287 the hydroxyl radical. *The Journal of Physical Chemistry A* 2002;106(19):4798-807.
- 288 [29]Valverde JM. On the negative activation energy for limestone calcination at high temperatures nearby
289 equilibrium. *ChEnS* 2015;132:169-77.
- 290 [30]Bhunia A, Bansal K, Henini M, Alshammari MS, Datta S. Negative activation energy and dielectric
291 signatures of excitons and excitonic Mott transitions in quantum confined laser structures. *JAP*
292 2016;120(14):144304.
- 293 [31]Wang Y, Widmann D, Wittmann M, Lehnert F, Gu D, Schüth F, et al. High activity and negative
294 apparent activation energy in low-temperature CO oxidation—present on Au/Mg (OH) 2, absent on
295 Au/TiO 2. *Catalysis Science & Technology* 2017;7(18):4145-61.